Oscillatory behavior in the electrical resistivity of transition-metal superlattices

Sihong Kim and Ivan K. Schuller
Physics Department 0319, University of California at San Diego, La Jolla, California 92093-0319
(Received 25 September 1997; revised manuscript received 8 January 1998)

The electrical resistivity of Co/Ni and Cu/Ni superlattices exhibit resistivity oscillations as a function of superlattice period Λ, while Ag/Pd does not. Moreover, the resistivity of Co/Ni superlattices shows quantum size effects and a resistivity enhancement with Λ, as a function of total film thickness d. These results are consistent with a model which assumes d-electron localization in the superlattice structure. [S0163-1829(98)04227-1]

I. INTRODUCTION

The transport properties of transition-metal multilayers have received renewed interest since the discovery of giant magnetoresistance (GMR),[1] followed by the oscillatory coupling between ferromagnetic layers.[2,3] Such artificially layered structures enable us to explore unique properties, otherwise unobservable in nature. The term multilayer, or superlattice, generally refers to thin films made by the sequential deposition of more than one material. Although the terms are often used interchangeably, it is customary to label the material as a superlattice if crystalline coherence, normal to the layers, is maintained over a distance longer than the modulation period, whereas if this additional ordering is absent, the term multilayer is preferred.[4]

Semiconductor superlattices have been found to exhibit interesting phenomena due to the quantum-well states created by the band edges in these films.[5] Observation of resonance Raman scattering,[6] Shubnikov–de Haas oscillations,[7] phonon folding,[8] electron localization in a two-dimensional electron gas,[9] and tunneling cyclotron resonance[10] are only a few examples. But such phenomena have rarely been observed in metallic films. Only recently have quantum-well states been observed in metallic films using photoemission spectroscopy.[11]

Recently, we showed that Co/Ni (fcc/fcc) superlattices fabricated by ultrahigh vacuum molecular-beam epitaxy (MBE) (Ref. 12) form coherent superlattice structures along the growth direction throughout the entire film thickness. A coherent electronic wave function, over many superlattice periods, in such a superlattice may exhibit interesting electronic properties unique to superlattices (''*superlattice effect.*'') A recent report on resistivity oscillations in these films[13] may be such an example. It has been suggested that this oscillatory behavior may indicate the presence of a scattering process existing only in superlattices. A proposed model, based on localized d electrons in slightly perturbed superlattice potential, seems consistent with the published data.[14] Therefore, it is necessary to investigate this oscillatory behavior in superlattices other than Co/Ni. In this paper, we (1) present transport data to help understand this behavior, (2) analyze experimental data available so far, and (3) expand the proposed localization model to transition-metal superlattices in general.

In Sec. II, fabrication and resistivity measurement of two other transition-metal superlattices, Cu/Ni and Ag/Pd, are discussed. Cu/Ni shows similar oscillatory behavior, whereas Ag/Pd does not. In Sec. III, a series of Co/Ni superlattices, with varying number of bilayers (i.e., total film thickness), are investigated to study the evolution of the *superlattice effect*. Resistivity measurements when compared to known scattering processes in thin metallic films imply the presence of a scattering process in these superlattices. In Sec. IV, available experimental data are summarized and compared with various available models. In Sec. V, the localization model, applied earlier to Co/Ni,[14] is expanded to Cu/Ni and Ag/Pd superlattices. The implication of the model is also discussed.

II. Cu/Ni AND Ag/Pd SUPERLATTICES

It is of interest to investigate if the low-temperature resistivity oscillations, observed in Co/Ni superlattices,[14] are observable in other superlattices. Cu/Ni is a good candidate because it is next to the Co/Ni pair in the Periodic Table. However, it should be recalled that Co and Ni are ferromagnetic materials whereas Cu is not, because of its completely filled $3d$ band. Ag/Pd is also chosen for investigation because the importance of d electrons has been suggested.[14] Ag/Pd formed from nonmagnetic elements is just below the Cu/Ni pair in the periodic table and have completely filled d bands.

A. Film growth and characterization

Epitaxial Cu/Ni (fcc/fcc) superlattices were grown by molecular-beam epitaxy (MBE) along the [111] direction on single-crystal [11.0] sapphire substrates. Film growth and structural characterization methods were similar to those used for the Co/Ni superlattice.[14] A 50 Å Co buffer layer was grown at 300 °C and subsequently annealed at 550 °C for 15 min prior to the deposition of the Cu/Ni superlattices. The substrate temperature during the superlattice growth was reduced to 120 °C to minimize alloy formation at the interface without deteriorating the crystalline quality of the film. An alloy film was also prepared via co-evaporation of Cu and Ni for comparison. All films have the same ratio of Cu to Ni atomic planes in each bilayer, denoted as $(Cu_{0.4\Lambda}Ni_{0.6\Lambda})_N$, where Λ is the superlattice period. The number of bilayers N in each film was adjusted such that the total thickness of the

film was ~1000 Å. The same superlattice configuration has been used for Co/Ni superlattices in Ref. 14.

Epitaxial Ag/Pd (fcc/fcc) superlattices were grown by MBE along the [111] direction on single-crystal [00.1] sapphire substrates. Electron-beam evaporation was used for Pd whereas Ag was evaporated from a Knudsen effusion cell at 950 °C. The evaporation rate was ~0.2 Å/sec for Pd and ~0.36 Å/sec for Ag. A 100 Å Pd buffer layer was grown at 500 °C and then the substrate temperature was reduced to 200 °C during the superlattice growth. The optimum growth parameters for Ag/Pd superlattices are harder to find than Co/Ni or Cu/Ni. First, Ag and Pd have a relatively large lattice mismatch (~5.6%), suggesting highly strained interfaces in the superlattice structure. Second, the melting points are quite different, 1827 K for Pd and 1235 K for Ag, which makes it difficult for the optimization of the growth temperature. Third, the formation of interfacial Ag-Pd alloys complicates data interpretation. The residual resistivity of Ag-Pd alloys depends strongly on concentration[15] exhibiting a maximum value of ~40 $\mu\Omega$ at 40 at. % of Ag.[15] Fourth, interdiffusion estimated from auger electron spectroscopy (AES) at the Ag/Pd interface was larger (>20 Å) than at Cu/Ni (~9 Å) or Co/Ni (~5 Å) interface. Therefore, the Ag layer thickness is kept constant while varying the Pd thickness, instead of keeping the Ag to Pd thickness ratio constant as was done for Cu/Ni. This way, the relative Pd concentration changes monotonically, in spite of small fluctuations in the evaporation rate for the Ag or Pd. Therefore, fluctuation in background resistivity, due to either interface scattering or alloy phase, which may mimic an oscillatory behavior, can be avoided. The Ag thickness was kept constant at ~23 Å for all superlattice films and the Pd thickness was varied from 5 Å to 55 Å. The number of bilayers was adjusted to make the total film thickness ~1000 Å. A 1000 Å thick Pd film was also prepared for comparison. We should stress that Ag/Pd resistivity oscillations would be observable in this configuration as well as shown earlier for Co/Ni as a function of either Co or Ni thickness.[13]

Figures 1 and 2 show *in situ* reflection high-energy electron diffraction (RHEED) patterns of Cu/Ni and Ag/Pd superlattices. Co [Fig. 1(a)], and Pd [Fig. 2(a)] buffer layers, grown on sapphire substrates, show sharp streak patterns, typical for a smooth surface. A typical RHEED pattern from a Ni-terminated surface of completed Cu/Ni [Fig. 1(b)] is similar to the one from Co/Ni, indicating similar epitaxial growth and structure in Cu/Ni and Co/Ni. On the other hand, the diffraction profile for a Pd-terminated surface of completed Ag/Pd [Fig. 2(b)] is not as sharp as the one from Cu/Ni, indicating a slightly worse epitaxial growth of Ag/Pd as mentioned above.

Layered structure of the films was further analyzed, *ex situ*, using x-ray diffraction (XRD). Figure 3 shows the θ–2θ XRD spectra of (a) Cu/Ni and (b) Ag/Pd. In Cu/Ni, the superlattice satellite peaks near the Cu/Ni[111] Bragg peak were clearly observed. Even the sample with $\Lambda=10$ Å, which has ~2 Cu and ~3 Ni atomic layers in each superlattice period, shows superlattice peaks, indicating a well-defined layered structure. In Ag/Pd, the XRD spectra look complicated due to the presence of the Pd [111] buffer Bragg peak. The shift of the average [111] Bragg peak of Ag/Pd is noticeable due to a large lattice mismatch [see the arrows in

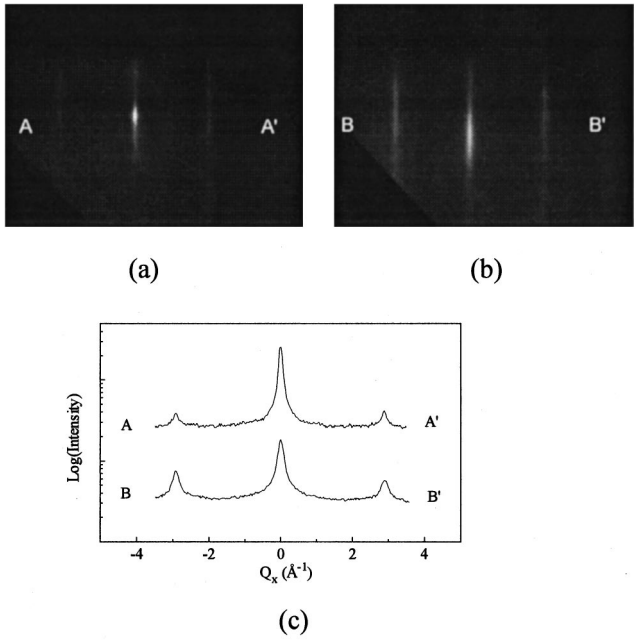

FIG. 1. RHEED pattern of typical Cu/Ni superlattices. (a) 50 Å thick Co buffer layer. (b) 1000 Å thick superlattice film terminated by Ni. (c) Diffraction peak profile across the lines labeled.

Fig. 3(b), indicating the Ag[111] and Pd[111] Bragg peak position]. All superlattice films, except Pd thickness ~5 Å, showed superlattice peaks associated with Λ. This indicates that Ag/Pd has a well-defined, at least chemically modulated, layered structure despite the larger interdiffusion. The presence of superlattice peaks of Cu/Ni at $\Lambda=10$ Å and an unobserved superlattice peak of Ag/Pd at Pd thickness=5 Å, is consistent with the estimate of the interdiffusion region near the interfaces from AES. The growth of a Ag/Pd superlattice

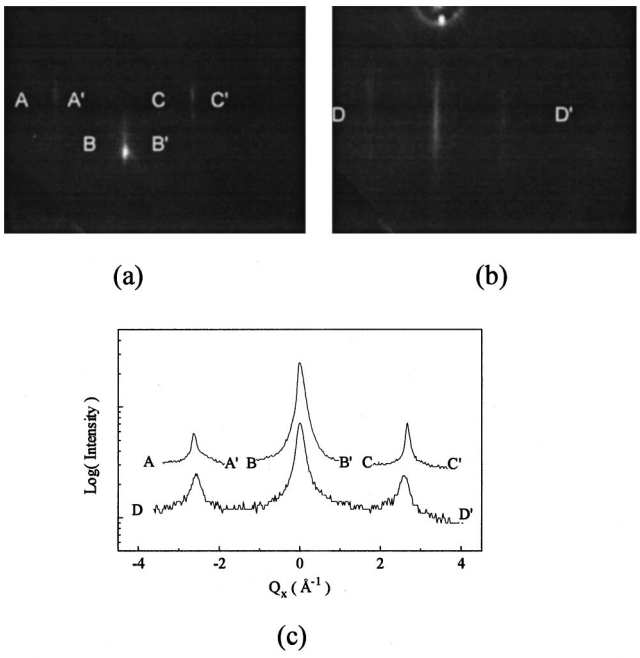

FIG. 2. RHEED pattern of typical Ag/Pd superlattices. (a) 100 Å thick Pd buffer layer. (b) 1000 Å thick superlattice film terminated by Pd. (c) Diffraction peak profile across the line labeled.

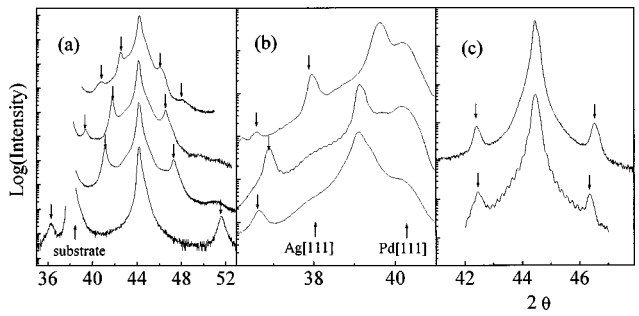

FIG. 3. High angle x-ray diffraction spectra of Cu/Ni, Ag/Pd, and Co/Ni superlattices. From the top figure, (a) $Cu_{22\,Å}/Ni_{33\,Å}$, $Cu_{16\,Å}/Ni_{24\,Å}$, $Cu_{12\,Å}/Ni_{18\,Å}$, $Cu_{4\,Å}/Ni_{6\,Å}$, (b) $Ag_{23\,Å}/Pd_{40\,Å}$, $Ag_{23\,Å}/Pd_{20\,Å}$, $Ag_{23\,Å}/Pd_{15\,Å}$, (c) $(Co_{20\,Å}/Ni_{28\,Å})_{23}$, $(Co_{20\,Å}/Ni_{30\,Å})_{10}$. The arrows indicate satellite peaks associated with superlattice modulation. Note that ~960 Å thick $Ag_{23\,Å}/Pd_{20\,Å}$ and ~550 Å thick Co/Ni shows finite-size peaks as well.

film has an interesting peculiarity that, at a particular modulation period (Pd thickness ~20 Å and Ag ~23 Å), very sharp finite-size peaks, due to the interference between the top and bottom surface of the film, are clearly observed [middle figure in Fig. 3(b)], suggesting very flat interfaces. In general, finite-size peaks are hardly observed for 1000 Å thick films because of instrumental resolution. For example, in commonly used Cu K_α radiation in XRD, separation of $K_{\alpha 1}$ and $K_{\alpha 2}$ reflection peaks is close to that of finite-size peaks from ~900 Å thick films.

Typical XRD spectra of Co/Ni superlattices are also shown in Fig. 3(c) for comparison. The Co/Ni [111] Bragg peaks and superlattice peaks are clearly observed in Co/Ni films. A 550 Å thick film also shows finite-size peaks, suggesting that smooth interfaces are maintained for the entire film thickness. For 1000 Å thick films, finite-size peaks are not observed in Co/Ni. In short, our XRD, RHEED, and AES data consistently indicate that Cu/Ni and Ag/Pd superlattices have a modulated structure comparable to Co/Ni.

B. Electrical resistivity

The electrical resistivity was measured by a standard four probe method on photolithographically patterned samples.

Figure 4 is the 4.2 K resistivity of Cu/Ni as a function of (a) Λ^{-1} and (b) Λ. The resistivity of the Cu/Ni superlattices, like many other metallic multilayers,[19] increases with decreasing Λ due to interface scattering. In other words, ρ is proportional to the number of bilayers N for fixed overall thickness d (i.e., $\rho \sim N \sim d/\Lambda$). Figure 4(a) shows this linear behavior as has been observed by many authors.[16–19] However, two features can be easily recognized in Fig. 4. First, Fig. 4(b) shows small oscillations as observed in Co/Ni, superimposed on the monotonically decreasing background due to interface scattering. Reproducibility of the data was tested by preparing a few duplicate samples, which had the same resistivity within the error bars shown in the figure. In addition, in Fig. 4(a), interface scattering can be identified easily as the Λ^{-1} dependence, observed above 0.025 $Å^{-1}$ (i.e., Λ less than 40 Å), which extrapolates through the origin. This indicates that bulk scattering by structural defects, which contribute a constant background resistivity, can be neglected for Λ less than 40 Å. A small constant background

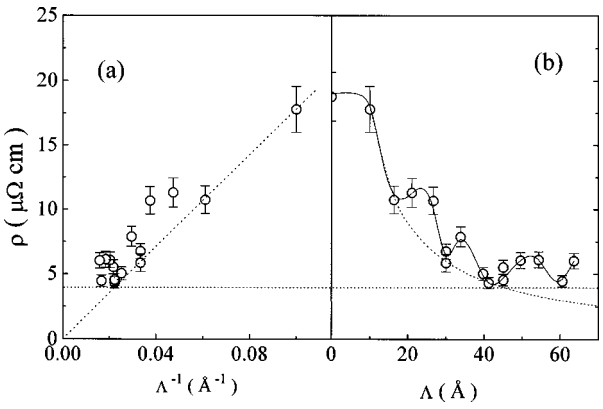

FIG. 4. 4.2 K resistivity of Cu/Ni superlattices as a function of (a) Λ^{-1} and (b) Λ. The dotted lines are the background resistivity discussed in text and the solid lines are guides to the eye.

resistivity (less than 4 $\mu\Omega$ cm), observed for $\Lambda \geq 40$ Å, may be due to perpendicular grain boundaries, as opposed to the Cu/Ni interfaces which are parallel to the interface. The oscillatory part of the resistivity, after removing the interface and grain boundary scattering contribution, is of about the same magnitude as Co/Ni (~2 $\mu\Omega$ cm). Large background resistivity might obscure this resistivity oscillations in Cu/Ni.

Figure 5 shows the 10 K resistivity of Ag/Pd superlattices. The overall resistivity is somewhat higher than for Co/Ni. There are no resistivity oscillations outside the experimental uncertainty. A small dip at a Pd thickness of ~20 Å (12% lower than the average of the neighboring data points) is significant. However, we believe that this can be explained otherwise, considering the difference in the microstructure of this particular film, as mentioned earlier. This is the only film which shows the finite-size peaks at high angle XRD [Fig. 3(b)]. The low angle XRD also shows very pronounced finite peaks which doubled the number of observable peaks (~40) in contrast to the neighboring films. The better crystalline structure of the film would reduce the resistivity because of less scattering from defects and grain boundaries. The resistivity of our films is consistently lower than the known Ag/Pd alloy resistivity at equivalent concentration.[15] The differences are larger than the experimental uncertainties. Therefore, the absence of oscillations may not be a direct

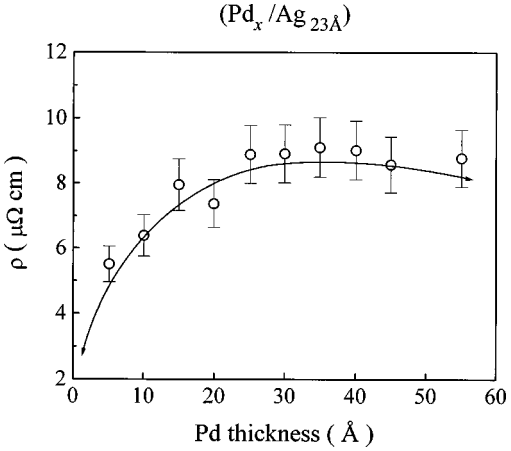

FIG. 5. 10 K resistivity of Ag/Pd superlattices as a function of Pd thickness. The solid line is a guide to the eye.

consequence of Ag/Pd alloys at the interfaces. Lack of apparent resistivity oscillations in Ag/Pd suggests the importance of the d electrons. Ag does not have any valence d electrons and Pd has only ~ 0.36 d holes.[20] In other words, the $4d$ band of Pd, which is nonmagnetic, is $\sim 96.4\%$ full. On the other hand, the $3d$ band of Ni, which is ferromagnetic, has ~ 0.6 holes and its minority spin band is only $\sim 88\%$ full.[20] Therefore, the Fermi level of Pd is much closer to the d-band edge. This may explain the difference between Ag/Pd and Cu/Ni or Co/Ni. More detailed discussion is given in Sec. VI.

III. SCATTERING PROCESSES IN METALLIC SUPERLATTICES

Among the three superlattice systems studied, Co/Ni and Cu/Ni show resistivity oscillations. However, Cu/Ni is not suitable for further study because of large interface scattering.[16–18] Therefore, in order to study various scattering processes present in thin metallic films, Co/Ni superlattice is a better choice.

The resistivity in the presence of several distinct scattering mechanisms is given, in its simplest form, by Mathiessen's rule:[21]

$$\rho = \rho_i + \rho_s(d) + \rho_{\text{inter}}(\Lambda) + \rho_{e\text{-ph}}(T) + \rho_{e\text{-}e}(T) + \rho_{\text{super}}, \tag{1}$$

where ρ_i is due to crystalline defects, chemical impurities, grain boundaries, etc., ρ_s is a size effect, ρ_{inter} is due to the interfaces, $\rho_{e\text{-ph}}(\rho_{e\text{-}e})$ is the resistivity due to electron-phonon (electron-electron) scattering, and ρ_{super} is a possible contribution associated with the superlattice structure. Each term has its own characteristic dependence on different parameters, such as superlattice period Λ, film thickness d, temperature T, etc. Therefore, by careful analysis, we can identify each mechanism one by one.

In Co/Ni superlattices, the additional contribution to the resistivity ρ_{super}, the focus of this paper, oscillates with individual layer thickness and/or superlattice period and is observable only in thick films.[13] It is natural to assume that $\rho_{\text{super}} = \rho_{\text{super}}(\Lambda, d)$. All other mechanisms are relatively well understood theoretically and have been observed experimentally in numerous systems.

Thus far, we have discussed[13,14] mainly the resistivity oscillations observed in thick films (~ 1000 Å). Now, we will focus on the dependence on the total film thickness. The electrical transport for very thin films is a complicated phenomenon because many different scattering mechanisms are involved which depend on the size of the film, such as the classical size effect (CSE),[22] the quantum size effect (QSE),[23] interface scattering,[24] grain boundary scattering,[25] etc. These mechanisms become significant when the film thickness is comparable to or less than the mean free path (MFP) of the electron. On the other hand, a *superlattice effect* should only be observed for a large number of layers, i.e., for thick films. Therefore, it is somewhat difficult to investigate the evolution of the superlattice effect with total film thickness. Careful film preparation, structural characterization, and a comprehensive understanding of the size effects are necessary to derive any meaningful conclusion.

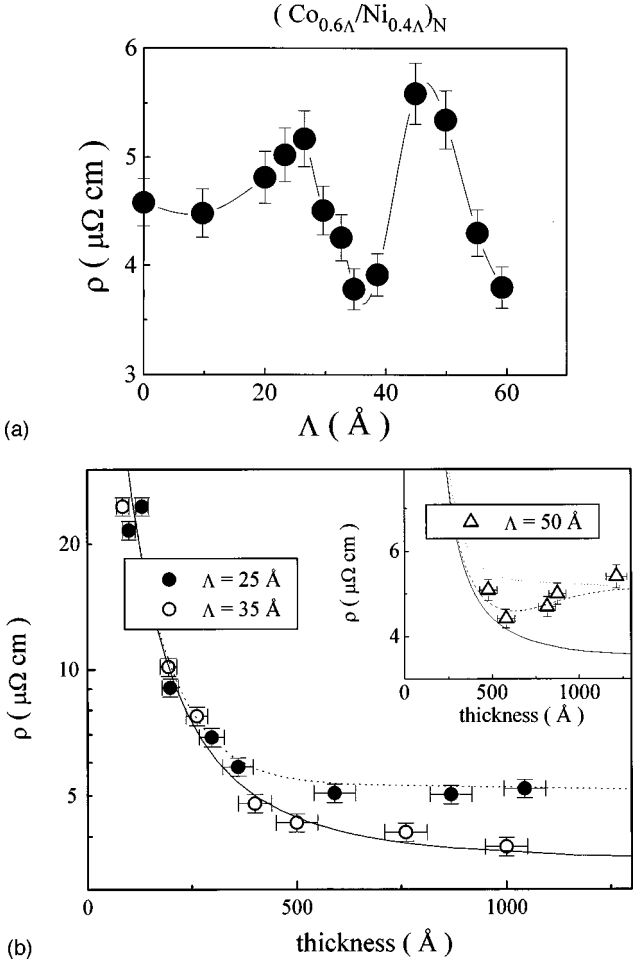

FIG. 6. (a) 4.2 K resistivity of $Co_{0.6\Lambda}/Ni_{0.4\Lambda}$ superlattices (~ 1000 Å thick, Ref. 14). (b) 4.2 K resistivity of Co/Ni at $\Lambda = 25$, 35, and 50 Å (inset) as a function of film thickness d. There is a resistivity minimum for $\Lambda = 50$ Å.

We will now focus on terms comprising the low-temperature residual resistivity. The negligible interface scattering in Co/Ni was already discussed in a previous paper.[14] Therefore, the low-temperature residual resistivity can be written as

$$\rho = \rho_i + \rho_s(d) + \rho_{\text{super}}(\Lambda, d). \tag{2}$$

Our previous report on resistivity oscillations in ~ 1000 Å thick Co/Ni superlattices of constant Co to Ni ratio (3:2) is reproduced in Fig. 6(a). We will now examine the change in resistivity with film thickness for fixed Λ's. Figure 6(b) shows the the thickness dependence of the resistivity at a resistivity maximum $\rho_{\max}$ ($\Lambda = 25$ Å) and resistivity minimum $\rho_{\min}$ ($\Lambda = 35$ Å). ρ becomes independent of Λ for film thickness d less than 300 Å ($\rho_{\max} \approx \rho_{\min}$). However, ρ is consistently higher in the $\Lambda = 25$ Å series for d greater than 300 Å ($\rho_{\max} > \rho_{\min}$). Since the resistivity difference is observed only for thick films (i.e., large number of bilayers N), this can be attributed to a *superlattice effect*. It is important to point out that this conclusion is only valid if the structure of the film does not change with thickness as proved by our detailed structure studies.[12,26]

Recently, a power law in surface conductivity, $\sigma_s \equiv 1/\rho_s \sim d^{2.3}$ was reported in thin $CoSi_2$ films and this was interpreted as a quantum size effect (QSE) (Ref. 23) due to the intersubband transitions induced by random potential fluctuation of a highly degenerate electron gas in a quantum box of thickness d. As a consequence, the resistivity in ultrathin films increases much faster than predicted by the classical size effect (CSE). The complete expression for the surface conductivity due to the QSE is given as[23]

$$\sigma_s \equiv 1/\rho_s = (e^2/\pi^5 h)(d^5/\lambda^2\Delta^2) \times 6/N(N+1)(2N+1)\sum_{\nu=1}^{N} k_{\nu_F}^2/\nu^2, \quad (3)$$

where e and h are the electron charge and Planck's constant, λ and Δ are the correlation length and the average range of a random potential fluctuation, N is the number of occupied subbands, and $k_{\nu p}$ is the Fermi wave vector of the νth band. This expression can be approximated by a power law for small d. This power law was claimed to be ''universal'' regardless of the realistic surface roughness because potential fluctuations on the atomic scale ($\lambda\Delta \sim 8$ Å) was enough to explain the sharp resistivity enhancement in $CoSi_2$.

In our case, σ_s follows the same power law, $\sigma_s \sim d^{2.3\pm0.2}$ for d less than 400 Å. If the free electron model is assumed with a carrier density $n \sim 5.4\times10^{22}/\mathrm{cm}^3$ [$\sim$0.6 s electron per atom in Co/Ni (Ref. 19)], then $\rho_{\min}$ ($\Lambda = 35$ Å) can be well described by the sum of ρ_i ($\sim 3.5\ \mu\Omega$ cm) and ρ_s due to QSE with $\lambda\Delta \sim 40\ \text{Å}^2$ [solid line in Fig. 6(b)]. In other words, an electronic MFP of $l \sim 260$ Å and a surface roughness of $\sim$10 Å. For $\rho_{\max}$ ($\Lambda = 25$ Å), the resistivity is enhanced, implying that an additional scattering effect is present, a *superlattice effect*.

If ρ_{super} increases with d at fixed Λ, then it would partially offset the diminishing surface scattering contribution ρ_s. Therefore, the resistivity, by proper choice of Λ, is expected to become nonmonotonic with d, which was indeed observed for the $\Lambda = 50$ Å samples [Fig. 6(b) inset]. It implies that the resistivity oscillates with Λ, but the oscillation amplitude may also depend on N. In other words, this effect becomes significant only if N exceeds a minimum number. Another interesting observation in Fig. 6 is that ρ_{super} is a bounded function, i.e., this effect does not grow with N without limit. This suggests that the crystalline coherence length of our films is limited by growth induced sources of additional scattering. The lines in Fig. 6(b) are generated with assumptions that ρ_{super} has an upper limit $\sim 2\ \mu\Omega$ cm and becomes significant when N exceeds $\sim$14 as implied by Fig. 6(b). These lines qualitatively describe the observed nonmonotonic data.

IV. SUMMARY OF EXPERIMENTAL DATA

It is useful to summarize all experimental findings before presenting our model.

(1) Low-temperature resistivity oscillations are observed in Co/Ni and Cu/Ni superlattices, but not in Ag/Pd superlattices. Therefore, this effect may require partially filled d bands in the constituent elements.

(2) The oscillations are above theoretical predictions implying the presence of an additional scattering mechanism.

(3) The oscillation amplitude does not change with temperature.[14] In other words, electron-phonon or electron-electron scattering processes are not significantly different in superlattices, suggesting that the electronic band structure, at least the conduction s band of majority charge carriers, is not significantly altered by the superlattice potential.

(4) The oscillation amplitude increases with a small amount of random fluctuation in the superlattice period.[14] This indicates that oscillations may be due to periodic perturbation from perfect superlattice symmetry.[14]

(5) The oscillations are observed as a function of individual layer thickness and/or superlattice period. The oscillation period does not depend on the size of the superlattice unit cell.[13,14]

The resistivity oscillations are the most intriguing observation since they cannot be explained by known scattering processes. It is very unlikely that random fluctuations of the data cause apparent oscillations. The oscillation amplitude is considerably outside experimental error and the resistivity of several duplicate samples were reproducible within the experimental error.

It is also unlikely that structural changes cause this oscillatory behavior. First, lattice strain at the interfaces is not likely oscillatory, unlike pseudomorphic growth on open surfaces.[27] Second, Ag/Pd superlattices, which would have a large strain due to a larger lattice mismatch than Co/Ni and Cu/Ni, shows no oscillations. Third, available structural data (XRD, RHEED, LEED) fail to reveal any correlation between resistivity oscillations and measurable parameters.

Oscillatory magnetic coupling (e.g., RKKY) might lead to resistivity oscillations. However, both Co and Ni are well-known ferromagnetic materials and measured magnetic properties, such as coercivity, saturation field, magnetic moment, or remnant magnetization, do not show oscillatory behavior. In addition, such oscillatory magnetic coupling would exist even in two or three bilayer samples. Therefore, it is unlikely.

Oscillatory behavior of electronic origin is a possibility. But this does not seem to be a density of states effect, such as the superlattice energy minigap model, as suggested in our earlier paper.[13] First, the temperature-dependent resistivity is almost sample independent.[14] In other words, the contribution from dynamic scattering mechanisms, such as electron-electron, electron-magnon, or electron-phonon scattering is similar in all samples, which should be affected by the presence of energy minigaps. Second, if the resistivity oscillations are caused by the energy minigaps at the Fermi level, their amplitude should decrease with increasing disorder as the modulation period becomes more diffuse, which is not what is observed experimentally.[14] Third, the proposed modification in $3d$ hole pockets around L sites of fcc Ni bands would not likely cause any significant change in the density of states at the Fermi level due to high symmetry.

Recently, Kiwi *et al.*[28] suggested that the resistivity oscillations are due to an additional scattering mechanism, not included in the band structure calculations. In their model the majority spin-up s electrons scatter resonantly against the mainly d-character quantum-well states induced in the Ni layers. Since this scattering is only effective when the

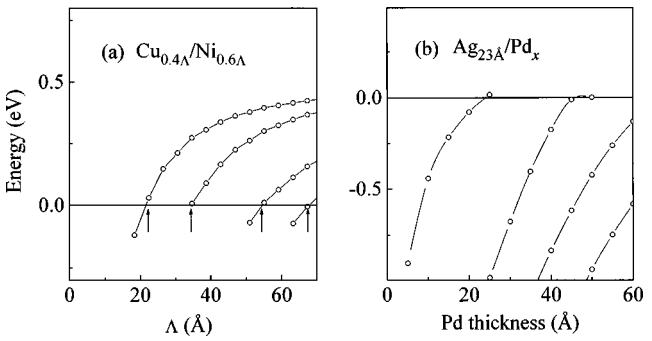

FIG. 7. Calculated energy eigenvalues of localized states of (a) $Cu_{0.4\Lambda}/Ni_{0.6\Lambda}$ and (b) $Ag_{23\,\text{Å}}/Pd_x$ superlattices. Energy is referenced from the Fermi level. Arrows indicate the positions of the resistivity maxima from Fig. 4(b).

quantum-well state energy is close to the Fermi level, and the former shift as a function of the layer thickness, oscillations in the resistivity result. However, the quantum-well state should exist in superlattices of any number of bilayers. It may be difficult to reconcile the experimental data with the fact that the oscillatory behavior disappears with decreasing number of bilayers. Nonetheless, this model shares similarities to our localization model.[14] It assumes the existence of an electronic state which periodically crosses the Fermi level, and an energy-dependent scattering cross section. The origin of these quantum-well states is a nondispersive minority *d* band in Ni along the Λ-*L* line, which happens to intersect the Fermi surface. Recent elaborate band structure calculations for the Co/Cu superlattices[29] have shown almost dispersionless localized bands with a predominantly *d* character. It is not yet clear whether such superlattice band structure calculations can be applied to real imperfect superlattices. However, it could be that in real superlattices these states become localized states, as suggested in Ref. 14.

The localization model was successful in explaining the resistivity oscillation maxima in Co/Ni superlattices,[14] and so far consistent with data summarized in the beginning of this section. In the following section, we expand our model to transition-metal superlattices in general and compare it with existing resistivity data.

V. LOCALIZATION MODEL

In superlattices, electrons experience a modulated potential due to alternating constituent elements. We propose that some of the *d* electrons are localized by this superlattice potential, which can be treated as a small perturbation on the perfectly periodic system and that there is a resonant scattering between the conduction *s* electrons and the localized *d* electrons. The scattering cross section is greatly enhanced when scattering occurs at the Fermi level. Because the energy eigenvalues of the localized states vary gradually with the superlattice potential, these states repeatedly appear close to the Fermi level. As a consequence, the value of the resistivity oscillates. This model is consistent with the experimental observations summarized in the previous section. First, localization of the *d* electrons is a consequence of coherent superlattice structure over many modulation periods. In other words, the localization is a *superlattice effect*. Second, random layer fluctuations will assist the localization.[30] Recently, a partial localization of Ni *d* states has been suggested to explain the narrowing of Ni L_α emission of Ag/Ni multilayer by x-ray emission spectroscopy.[31] Third, only *d* electrons can be localized because aperiodic perturbations in the superlattice potential are not strong enough to localize *s* electrons. Therefore, the density of states of the *s* electrons at the Fermi level is not significantly altered in this model. In fact, it has been shown that localized states can exist in a one-dimensional quasiperiodic system.[32]

Consider the following one-dimensional tight-binding Hamiltonian:

$$H=\sum_n \varepsilon_n|n\rangle\langle n|+v_{n,n-1}|n\rangle\langle n-1|+v_{n-1,n}|n-1\rangle\langle n|, \tag{4}$$

where $|i\rangle$ denotes a Wannier state localized around the *i*th site. This Hamiltonian describes the formation of a band from a single atomic orbital through nearest-neighbor interaction.

The eigenfunction of the Hamiltonian with the eigenvalue *E* can be written as

$$|\Psi\rangle=\sum_n f_n|n\rangle, \tag{5}$$

where f_n satisfies the recurrence relation,

$$v_{n,n-1}f_{n-1}+v_{n,n+1}f_{n+1}=(E-\varepsilon_n)f_n. \tag{6}$$

In superlattices, which are fabricated from two different atomic species (*a* and *b*), there are only two choices for ε_n, [$\varepsilon(a)$ or $\varepsilon(b)$], depending on site occupancy. Similarly for $v_{n,n+1}$, there are three choices [$v(aa)$, $v(bb)$, $v(ab)$], as described below,

$$\varepsilon(x)\equiv\langle n;x|H|n;x\rangle:x=a,b,$$

$$v(xy)\equiv\langle n;x|H|n+1;y\rangle:x,y=a,b, \tag{7}$$

where additional indices *x* and *y* were used to denote explicitly the type of atoms occupying the particular sites.

These parameters can be estimated from the band structure of each element *a* and *b*. $\varepsilon(a)$ and $\varepsilon(b)$ are the average of the energy eigenvalues in each energy band, and $v(aa)$ and $v(bb)$ are proportional to each energy bandwidth. $v(ab)$ is assumed to be the average of $v(aa)$ and $v(bb)$ for simplicity:

$$v(ab)=[v(aa)+v(bb)]/2,$$

$$v(a)\equiv v(aa),$$

$$v(b)\equiv v(bb). \tag{8}$$

It is very useful to divide the Hamiltonian into two parts, one periodic with respect to the average lattice, and the remaining aperiodic term due to superlattice modulation. It is also convenient to reference energies to

$$\varepsilon_{\mathrm{ref}} \equiv [\varepsilon(a)+\varepsilon(b)]/2 \tag{9}$$

and rescale them in units of

$$V_H \equiv [v(a)+v(b)]/2. \tag{10}$$

Therefore, Eq. (6) can be rewritten as

$$(1+\beta_{n+1}\nu)f_{n+1}+(1+\beta_n\nu)f_{n-1}=2(E-\tau_n\Delta)f_n, \tag{11}$$

where

$$E=(E-\varepsilon_{\mathrm{ref}})/2V_H,$$

$$\Delta=|[\varepsilon(a)-\varepsilon(b)]/4V_H|, \quad \nu=|[v(a)-v(b)]/2V_H|,$$

$$\tau_n=(\varepsilon_n-\varepsilon_{\mathrm{ref}})/2V_H/\Delta, \quad \beta_n=(v_{n,n-1}/V_H-1)/\nu, \tag{12}$$

where Δ is the relative amount of band separation, v is the relative difference in bandwidth of the two atomic species composing the superlattice, and τ_n and β_n are determined by the atomic sequence in the actual superlattice film. τ_n and β_n are $+1$ or -1, depending on the actual site occupancy. In order to simulate interface disorder inherent in real superlattices, a new parameter σ is introduced, which is the interface region where the τ_n's and β_n's are assumed to change from $+1$ to -1 or vice versa. Equation (11) quite generally describes any combination of transition-metal superlattices. If $\beta_n=0$, it is reduced to the Hamiltonian we used in the Co/Ni system in Ref. 14.

The parameters used in the model calculation are determined from the band structure calculations of each element.[34] Only the width of the d band and the position of the Fermi level are necessary for this calculation. The width of the Ni $3d$ minority band is $\sim$5 eV and the Cu $3d$ band is $\sim$3 eV. The center of the each band is displaced by 1 eV, with Ni closer to the Fermi level. On the other hand, the width of the Pd $4d$ band is $\sim$5 eV and the Ag $4d$ band is $\sim$3 eV, and they are displaced by 2.5 eV. Therefore, $\nu=0.25$, $\Delta=0.25$ for Cu/Ni, and $\nu=0.25$, $\Delta=0.625$ for Ag/Pd are used for the model calculation. The interface region is approximately four monolayers ($2\sigma=4$) for Cu/Ni and ten monolayers ($2\sigma=10$) for Ag/Pd, based on the AES measurements.

VI. DISCUSSION

Figure 7 shows the calculated localized energy spectra of (a) Cu/Ni and (b) Ag/Pd superlattices investigated in this paper. In Fig. 7(a), localized states of Cu/Ni appear close to the Fermi level at $\Lambda=\sim$23, $\sim$35, $\sim$55, and $\sim$67 Å, close to Λ where the resistivity maxima are observed in Fig. 4(b). A similar result has already been found in Co/Ni.[14] Considering the simplicity of the one-dimensional calculation, it is a remarkable agreement. The repeated crossing of the localized states through the Fermi level is clearly correlated with the periodic enhancement of the resistivity. The resistivity is enhanced because of the resonance scattering between this localized state and the conduction $4s$ electrons.

In Ag/Pd, the calculated localized state approaches to and stays near the Fermi level, because the Fermi level lies at the upper edge of the Pd $4d$ band. This is expected because in this one-dimensional model the allowed states should reside between the upper edge of the $4d$ Pd band and the lower edge of the $4d$ Ag band.[33] From the calculation it is not clear what happens to the state once it approaches the Fermi level (close to the band edge). However, it is interesting to note that the resistivity of Ag/Pd in Fig. 5 increases gradually until a Pd thickness $\approx$25 Å, where the first calculated localized state approaches the Fermi level. Note that the $4d$ band of Pd is almost filled ($\sim$97% full). Even a small charge transfer from the $5s$ band to the $4d$ band in Ag/Pd would raise the Fermi level enough so that all energy eigenstates would lie below the Fermi level. In fact, it has been shown that the $4d$ hole of Pd in Ag/Pd alloys is completely filled at $\sim$60 at. % of Ag concentration.[15]

The localized states provide a scattering mechanism similar to *resonant scattering*. Because these localized states exist inside the conduction band, they are similar to *virtual bound states*.[35] A close analogy can be found in the dilute transition-metal impurities in Cu.[36] The d electrons of the transition-metal impurities form a virtual bound state inside the conduction band of Cu. When transition metals (Sc to Ni), are dissolved in the host metal, the mean energy of the broadened impurity d band changes systematically in relation to the Fermi level of the host metal. When the center of the impurity d band coincides with the Fermi level, there is a resonance and hence a maximum scattering effect with the conduction electrons at the Fermi level. Thus the resistivity due to the impurities rises when going through the series to a broad maximum around Cr and then diminishes again.[36] This implies that the scattering cross section of the *virtual bound state* is energy dependent. The cross section is a maximum when the Fermi level lies just in the middle of this state and decreases with increasing or decreasing energy. For 1 at % Cr impurities in Cu, the residual resistivity increases by $\sim$20 $\mu\Omega$ cm when the *virtual bound state* at Cr site lies near the Fermi level. When Ni is substituted for Cr, the increase is only $\sim$1 $\mu\Omega$ cm because for Ni the *virtual bound state* lies well below the Fermi level.[35,36]

In our case, the increase in residual resistivity is $\sim$2 $\mu\Omega$ cm when the proposed localized state lies at the Fermi level. Since this localization occurs only along the superlattice growth direction, the effect here is much smaller than the three-dimensional case and the scattering cross section is expected to decay more quickly as a function of the energy difference between the localized state and the Fermi level.

VII. CONCLUSIONS

So far, all existing data from Co/Ni, Cu/Ni, and Pd/Ag superlattices are consistent with the localization model. However, we cannot rule out the simultaneous presence of resonant scattering due to quantum Hall states as predicted by Kiwi *et al.*[28] The calculated localized states appear close to the superlattice period where the resistivity exhibits maxima. More sophisticated models, which include multiple bands and three-dimensional crystal structures, are necessary to understand this phenomenon more quantitatively. The

fraction of *d* electrons which are localized and the size of the scattering cross section are still open issues. Recent development in superlattice band structure calculations and their generalization to the imperfect superlattices which can be fabricated with current technology, may improve the understanding of transport in metallic superlattices.

ACKNOWLEDGMENTS

We thank M. Kiwi, R. Ramírez, M. Weissmann, P. Levy, L. J. Sham, and R. C. Dynes for invaluable discussions. This work was supported by the Department of Energy.

[1] M. N. Baibich, J. M. Broto, A. Fert, F. Nguyen van Dau, F. Petroff, P. E. Etienne, G. Creuzet, A. Friedrich, and J. Chazelas, Phys. Rev. Lett. **61**, 2472 (1988).

[2] For an early claim of RKKY coupling in Cu/Ni, see W.-S. Zhou, H. K. Wong, J. R. Owers-Bradley, and W. P. Halperin, Physica B&C **108B+C**, 953 (1981); in Fe/Cr, see S. S. P. Parkin, Phys. Rev. Lett. **64**, 2304 (1990).

[3] J. Mathon, M. Villeret, and H. Itoh, Phys. Rev. B **52**, R6983 (1995).

[4] I. K. Schuller, Phys. Rev. Lett. **44**, 1597 (1980).

[5] See, for example, *Quantum Well and Superlattice Physics*, edited by G. H. Dohler and Joel N. Schulman (Bellingham, Washington, 1987).

[6] P. Manuel, G. A. Sai-Halasz, L. L. Chang, C. A. Chang, and L. Esaki, Phys. Rev. Lett. **37**, 1701 (1976).

[7] L. L. Chang, H. Sakaki, C. A. Chang, and L. Esaki, Phys. Rev. Lett. **38**, 1489 (1977).

[8] C. Colvard, R. Merlin, M. V. Klein, and A. C. Gossard, Phys. Rev. Lett. **45**, 298 (1980).

[9] D. C. Tsui, H. L. Störmer, and A. C. Gossard, Phys. Rev. Lett. **48**, 1559 (1982); for a recent review, see *Localization and Confinement of Electrons in Semiconductors*, edited by F. Kuchar, H. Heinrich, and G. Bauer (Springer-Verlag, Berlin, 1990).

[10] G. Brozak, E. A. de Andrada e Silva, L. J. Sham, F. DeRosa, P. Miceli, S. A. Schwarz, J. P. Harbison, L. T. Florez, and S. J. Allen, Jr., Phys. Rev. Lett. **64**, 471 (1990).

[11] J. E. Ortega and F. J. Himpsel, Phys. Rev. Lett. **69**, 844 (1992); T. Miller, A. Samsavar, G. E. Franklin, and T.-C. Chiang, *ibid.* **61**, 1404 (1988).

[12] J. M. Gallego, S. Kim, T. J. Moran, D. Lederman, and Ivan K. Schuller, Phys. Rev. B **51**, 2550 (1995).

[13] J. M. Gallego, D. Lederman, S. Kim, and Ivan K. Schuller, Phys. Rev. Lett. **74**, 4515 (1995).

[14] Sihong Kim, D. Lederman, J. M. Gallego, and Ivan K. Schuller, Phys. Rev. B **54**, R5291 (1996).

[15] See, for example, J. S. Dugdale, *The Electrical Properties of Metals and Alloys* (Edward Arnold, London, 1977), pp. 269–279.

[16] H. Sato, T. Matsudai, W. Abdul-Razzaq, C. Fierz, and P. A. Schroeder, J. Phys.: Condens. Matter **6**, 6151 (1994).

[17] T. Sasaki, T. Kaneko, M. Sajuda, and R. Yamamoto, MRS Int'l. Mtg. Adv. Mats. **10**, 575 (1989).

[18] G. Reiss, K. Kapfberger, G. Meier, J. Vancea, and H. Hoffmann, J. Phys.: Condens. Matter **3**, 1257 (1989).

[19] I. K. Schuller and C. M. Falco, in *Inhomogeneous Superconductors*, AIP Conf. Proc. No. 58, edited by D. U. Gubser *et al.* (AIP, New York, 1979), p. 197.

[20] D. A. Papaconstantopoulos, *Handbook of the Band Structure of Elemental Solids* (Plenum, New York, 1986).

[21] See, for example, Claus Hamann, Hubert Burghardt, and Thomas Frauenheim, *Electrical Conduction Mechanisms in Solids* (VEB Deutscher Verlag der Wissenschaften, Berlin, 1988), Chap. 5.

[22] K. Fuchs, Proc. Cambridge Philos. Soc. **34**, 100 (1938); E. H. Sondheimer, Adv. Phys. **1**, 1 (1952).

[23] G. Fishman and D. Caleki, Phys. Rev. Lett. **62**, 1302 (1989); J. Y. Duboz, P. A. Badoz, E. Rosencher, J. Henz, M. Ospelt, H. von Känel, and A. Griggs, Appl. Phys. Lett. **53**, 788 (1988).

[24] R. Dimmich, J. Phys. F **15**, 2477 (1985).

[25] A. F. Mayadas and M. Shatzkes, Phys. Rev. B **1**, 1382 (1970).

[26] Sihong Kim, Harry Suhl, and Ivan K. Schuller, Phys. Rev. Lett. **78**, 322 (1997).

[27] J. Fassbender, U. May, B. Schirmar, R. M. Jungblut, B. Hillebrands, and G. Güntherodt, Phys. Rev. Lett. **75**, 4476 (1995).

[28] M. Kiwi, A. M. Llois, R. Ramírez, and M. Weissmann, Phys. Rev. B **54**, 15 335 (1996).

[29] J. L. Pérez-Díaz and M. C. Muñoz, Phys. Rev. Lett. **76**, 4967 (1996).

[30] K. Mader, L. Wang, and A. Zunger, Phys. Rev. Lett. **74**, 2555 (1995).

[31] P. Jonnard, F. Vergand, C. Bonnelle, and K. F. Badawi, J. Appl. Phys. **77**, 6044 (1995).

[32] For a review, see J. B. Sokoloff, Phys. Rep. **126**, 189 (1985).

[33] E. N. Economou and M. H. Cohen, Phys. Rev. B **4**, 396 (1971).

[34] J. L. Pérez-Díaz and M. C. Muñoz, Phys. Rev. B **50**, 8824 (1994); J. R. Anderson, D. A. Papaconstantopoulos, L. L. Boyer, and J. E. Schirber, *ibid.* **20**, 3172 (1979).

[35] See, for example, J. S. Dugdale, *The Electrical Properties of Metals and Alloys* (Edward Arnold, London, 1977), Chap. 7; G. Lehmann and P. Ziesche, *Electronic Properties of Metals* (Elsevier, Amsterdam, 1990), Chap. 5.

[36] I. Mertig, E. Mrosan, and R. Schopke, J. Phys. F **12**, 1689 (1982).